# *Chapter IV*

# *Adsorption using Treated Camellia sinensis stem (TCSS)*

## Chapter IV

# Adsorption using Treated *Camellia sinensis* Stem (TCSS)

Sorption characteristics of treated *Camellia sinensis* stem (TCSS) in the chelation of $PO_4^{3-}$, $NO_3^-$ and $SO_4^{2-}$ anions from aqueous solutions under variable operating factor are described in this chapter.

### 4.1 Microscopic Studies

Particle sizes of the raw and treated CSS were calculated through longitudinal and latitudinal measurements of granular mesh size imaged through microscope, (figure 4.1a & b) subjected to application of multiplication factor, followed by averaging the values. As per the results, the values particle sizes with reference to mesh sizes are listed in Table 4.1.

**Table 4.1 Mesh Sizes / Particle Sizes**

| Mesh Sizes (BSS) | Particle Sizes (mm) |
|---|---|
| 85 | 0.18 |
| 72 | 0.21 |
| 52 | 0.30 |
| 36 | 0.42 |
| 22 | 0.71 |

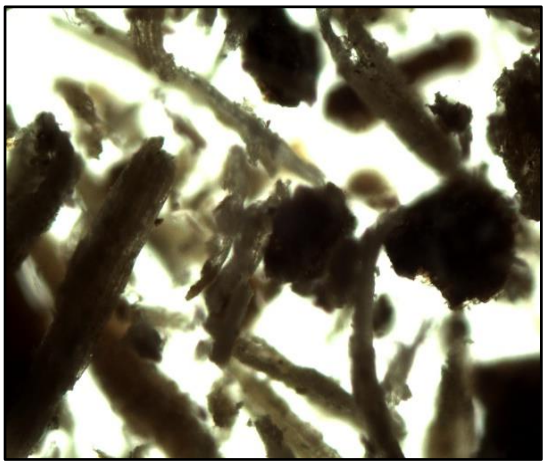

**Figure 4.1 a Raw CSS (0.18 mm)**

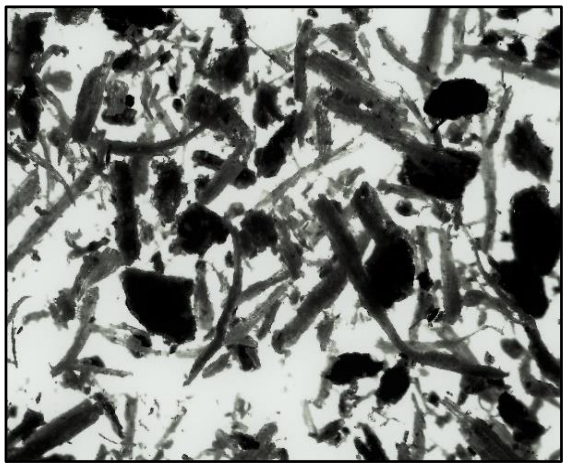

**Figure 4.1 b Treated CSS (0.18 mm)**

## 4.2 Physio- Chemical Characterization

Physio - Chemical parametric values of treated *Camellia sinensis* stem (TCSS – 0.18 mm) are listed in Table 4.2.

**Table 4.2 Physio- Chemical Characteristics**

| Properties | TCSS (0.18 mm) |
|---|---|
| pH of 1 % solution | 6.52 |
| Conductivity(mV) | 35.50 |
| Moisture (%) | 1.64 |
| Bulk density (g/L) | 0.65 |
| Specific gravity | 1.37 |
| Porosity | 55.59 |
| Ash content (%) | 3.29 |
| Acid Soluble Matter (%) | 2.16 |
| Water Soluble Matter (%) | 1.32 |
| Ion Exchange Capacity ($m_{eq}$ /g) | 0.47 |
| $pH_{zpc}$ | 5.13 |
| Surface area ($m^2$/g) | 36.31 |
| Mean Pore volume (nm) | 2.5 |
| Carbon (%) | 45.78 |
| Nitrogen (%) | 1.92 |
| Hydrogen (%) | 6.54 |
| Sulphur (%) | 0.24 |
| **Surface Acidic groups (m mol $g^{-1}$)** | |
| Phenolic | 0.63 |
| Carboxylic | 1.58 |
| Lactonic | 0.14 |

TCSS exhibited almost neutral pH value and lower moisture content value indicative of its stable nature[1]. The calculated bulk density less than 1 g/L implies the presence of porous particles as evident from standard porosity value and appreciable surface area/ mean pore diameter values derived from BET/ BJH plots (figs 4.2, 4.3). Internal pore structure mostly decides the extent of adsorption for any material. Pore size distribution with 0.1 – 1 nm, 1 – 10 nm and 10 – 100 nm refer to microporous, mesoporous and macroporous nature of the material as per IUPAC[2]. BET analysis provided precise surface area (36.31 $m^2/g$) as calculated from the following equation, analysed by nitrogen multilayer adsorption measured as a function of relative pressure using an automated analyser.

$$SA = X_m L_{av} A_m / M_v$$

where,

$L_{av}$ – Avogadro's Number ($6.02 * 10^{23}$)

$A_m$ – Cross sectional area of the adsorbate (0.162 $nm^2$ for the adsorbed nitrogen molecule)

$M_v$ – Molar volume (22414 mL)

Adsorption capacity ($X_m$) was calculated from positive slope value and intercept of the linear BET plot[2]. BJH analysis was employed to determine pore size distribution and specific pore volume. This technique characterizes pore size distribution independent of external area due to particle size of the sample[3]. The centred peak of BJH plot indicate the pore diameter of the sample as 2.5 nm, implying mesoporous nature.

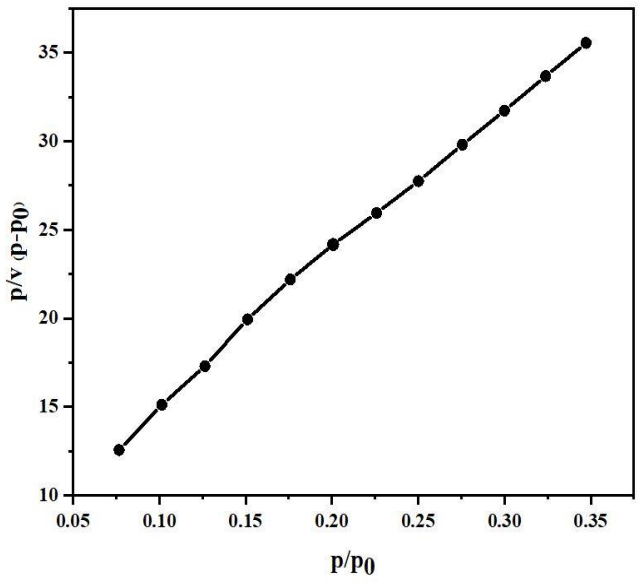


**Figure 4.2 BET Plot**

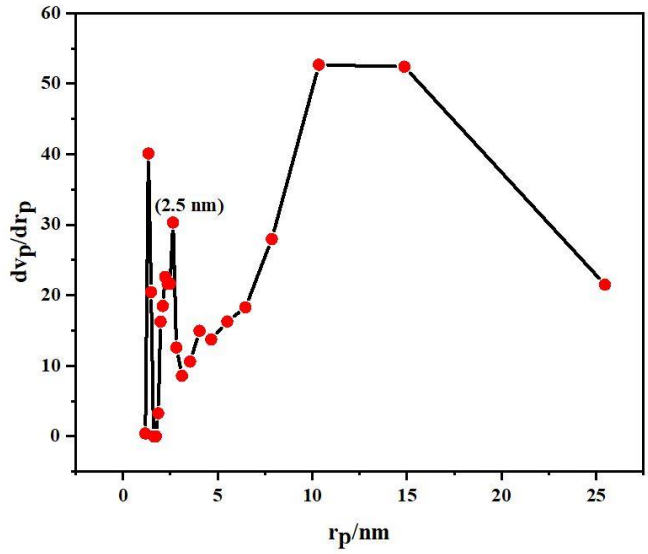


**Figure 4.3 BJH Plot**

Figure 4.4 depicts a typical $N_2$ sorption isotherm indicative of type IV hysteresis loop observed between the lower adsorption and upper desorption curves, which may be due to capillary condensation, favouring the presence of mesopores[4].

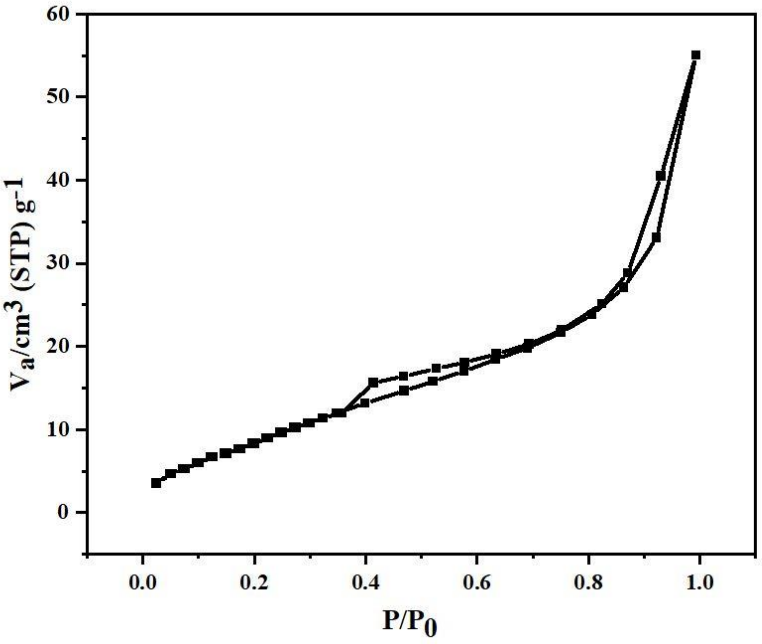


**Figure 4.4 Adsorption/ Desorption Isothermal Plot**

Specific gravity, less than 2, suggest marked sequestering property of the sample. Lower ash content value reflects on the presence of high carbon content in preference to other elements against inorganic matter[5]. Minimum water soluble/acid soluble matter values register lesser amount of sample impurity. The calculated values of $pH_{zpc}$ being less than native pH, show the involvement of greater number of $H^+$ ions leaving behind positively charged vacant sites[6]. This statement is supported by greater value of carboxylic group amongst the surface acidic groups studied.

Comparison of three specific parametric values (table 4.3) is made with other bio-sorbents reported earlier. It is understood from the tabular columns TCSS exhibit lesser ash content and moisture percentage which suffice enhanced active sites / stable nature. Also, lower bulk density value support greater exteriority with many pores.

**Table 4.3 Material Characteristics vs Literature Report – A Comparison**

| Adsorbents | Ash Content (%) | Bulk Density (g/L) | Moisture (%) |
|---|---|---|---|
| Tea waste[7] | 4.8 | 0.34 | 6.4 |
| *Moringa oleifera* bark[8] | 11.1 | 3.7 | 7.5 |
| Apple peel[9] | 7.4 | 2.4 | 12.2 |
| Wheat straw[10] | 7.7 | 1.8 | 6.7 |
| Corn Stalks[11] | 6.4 | 2.7 | 8.8 |
| *Camellia sinensis* stem (current study) | **3.29** | **0.65** | **1.64** |

## 4.3 SEM and EDAX Analyses

Information drawn from SEM images are as follows, heterogenous surface with aggregate particles (fig 4.5) was found to undergo surface morphological changes with opened pores due to chemical modification (fig 4.6). Smoothening of unoccupied pores after the experimental run with respective anions reflect homogenous structures instead of porous nature (figs 4.7- 4.9) facilitating the adsorption of anions[12].

Presence of $PO_4^{3-}$, $NO_3^-$ and $SO_4^{2-}$ anions peaks at 1- 3 keV substantiate the adsorption on TCSS (figs 4.11 - 4.13) against their absence in the unloaded spectra (fig 4.10).

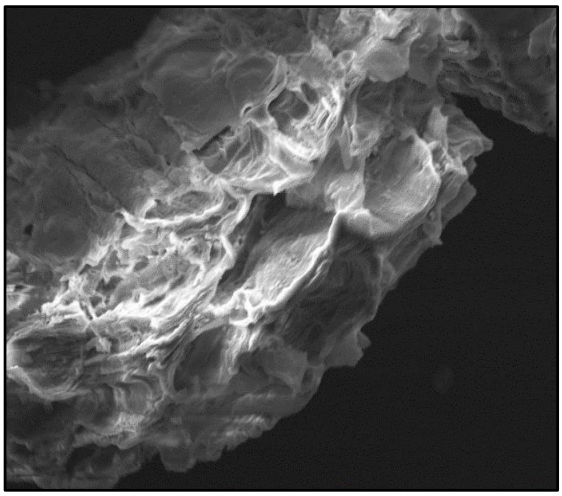

**Figure 4.5 Raw CSS**

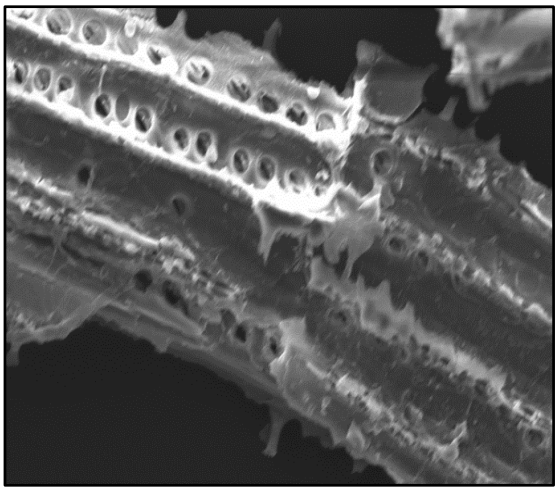

**Figure 4.6 Unloaded TCSS**

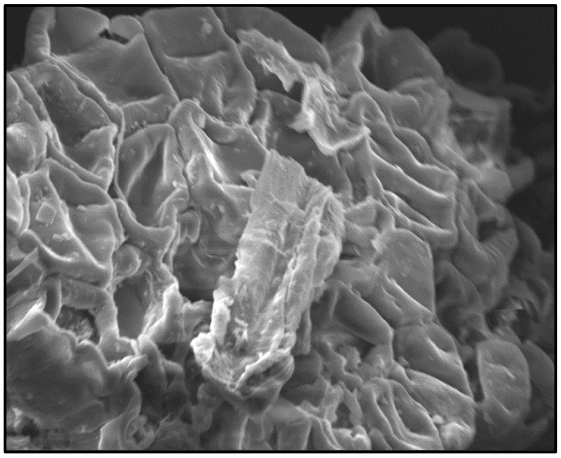

**Figure 4.7 $PO_4^{3-}$ loaded TCSS**

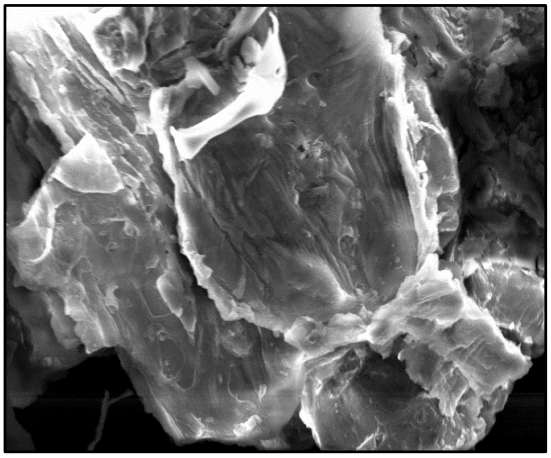

**Figure 4.8 $NO_3^-$ - loaded TCSS**

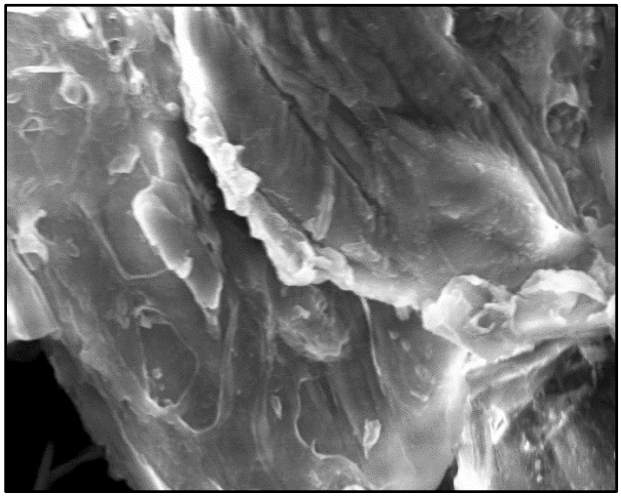

**Figure 4.9 $SO_4^{2-}$ - loaded TCSS**

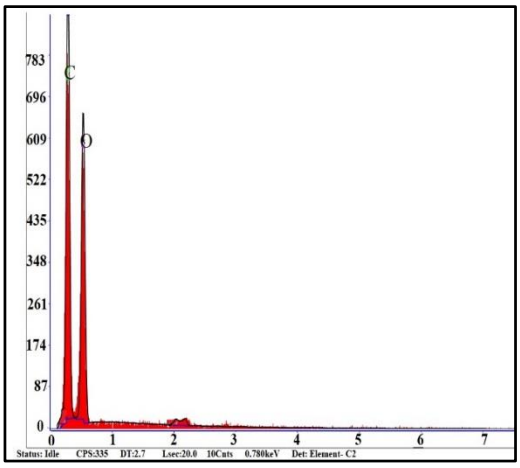


**Figure 4.10 Unloaded TCSS**

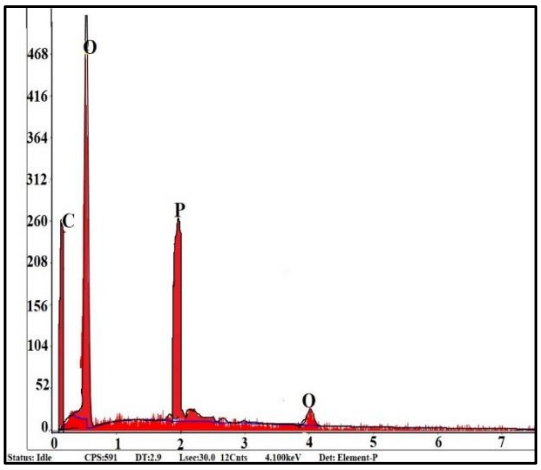


**Figure 4.11 $PO_4^{3-}$ loaded TCSS**

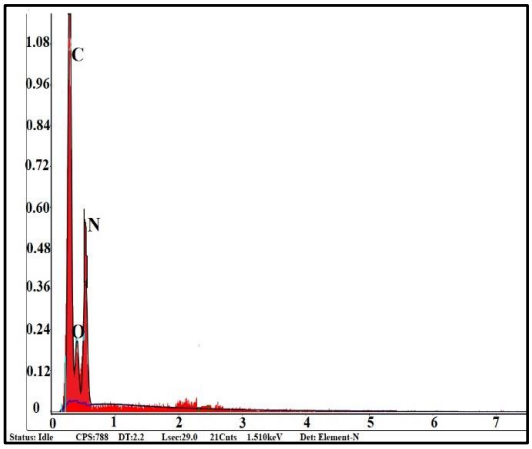


**Figure 4.12 $NO_3^-$ - loaded TCSS**

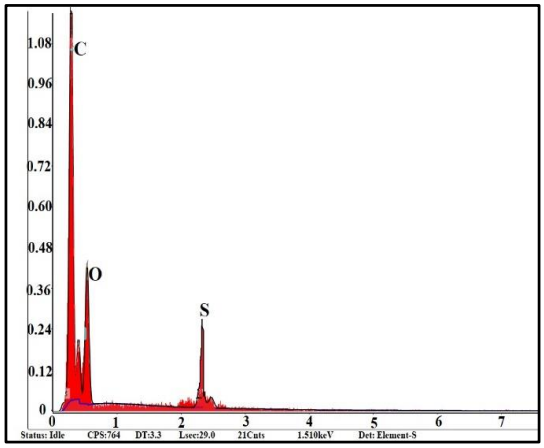


**Figure 4.13 $SO_4^{2-}$ - loaded TCSS**

## 4.4 FT-IR Spectral Studies

Unloaded TCSS (fig 4.14 a) shows peaks corresponding to O-H (3747 $cm^{-1}$), C=O (1646 $cm^{-1}$) functional groups C-H (1475 $cm^{-1}$) and C-O (883 $cm^{-1}$) stretching vibrations respectively[13]. The sorption bands (fig 4.14 b) at 3773 $cm^{-1}$ and 2924 $cm^{-1}$ refer to O-H and C-H stretching of carboxyl group and alkane respectively. It is inferred from the prominent peaks at, 2378 $cm^{-1}$ and 1518 $cm^{-1}$, the involvement of C=C alkyne and amide stretching. The characteristic peak at 998 $cm^{-1}$ is imply P-O stretching vibration, indicative of phosphate sorption onto TCSS[14]. A peak at 1032 $cm^{-1}$ (fig 4.14 c) in nitrate loaded spectrum, indicates N-O stretching, evidencing the sequestration of $NO_3^-$ ions by the modified material[15]. As per infrared analysis, 800 -1000 $cm^{-1}$ region is assigned to S-O

stretching[16]. Therefore, the peak observed (fig 4.14 d) at 867 $cm^{-1}$ is an accordance with the above statement, wherein the sorption of sulphate anion is obvious. Overall peak shifts, show the participation of functional groups present in the biomass surface during anion binding process.

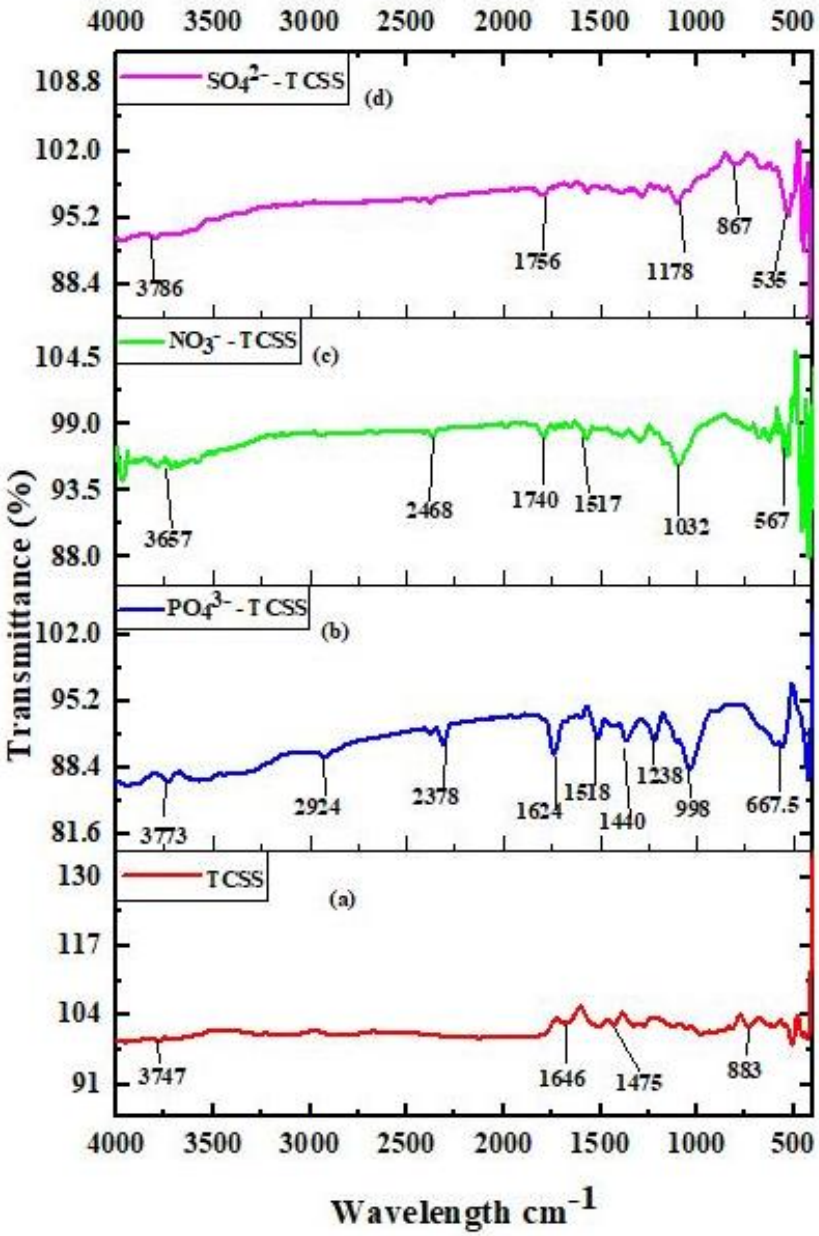


**Figure 4.14 FT-IR Spectra**

## 4.5 Batch Equilibration Experiments

### 4.5.1 Impact of Particle Size

Figure 4.15 registers maximum sorption capacity of TCSS for all the verified systems at a smaller particle size (0.18 mm) offering larger surface area for enhanced removal of anions[17]. Minimal sorption at increasing particle sizes could be due to the appreciable diffusional resistance to mass transport, wherein maximum internal surface is least utilized for adsorption. Similar observations were made by Monoj Kumar Mondal et al., and Lahieb Faisal Muhaisen et al., while employing rice husk/fruit juice residue and lemon peel as sorbent materials[18,19].

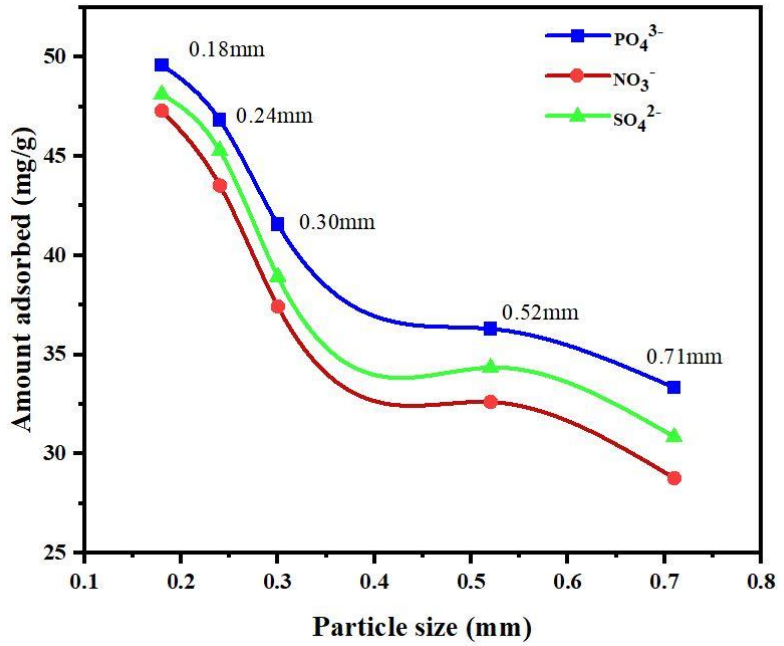


**Fig: 4.15 Impact of Particle size**

### 4.5.2 Impact of Initial Concentration and Agitation Time

Initial concentration of any sorbate species plays a key role during an agitation experiment in the determination of sorbents' sorption capacity[20]. Figures 4.16 and 4.17 (plotted as per the values listed in table 4.4) registered 49.26 mg/g and 46.92 mg/g adsorption capacity of TCSS for $PO_4^{3-}$/ $NO_3^-$ chelation by 100 mg/L initial anion concentration, whereas, figure 4.18 showed a maximum of 47.95 mg/g sorption capacity by the material for $SO_4^{2-}$ uptake at an initial concentration of 250 mg/L. All the three

graphs, recorded a diminishing anion sorption beyond the maximum sorption, which may be due to saturation of binding sites on the biomass surface leading to increased number of unadsorbed ions from the aqueous solution. Also, the curve pattern implies that the highest sorption had occurred at 10 mins, which favour the existence of numerous vacant sites upto the time frame of 10 minutes. A significant repulsive force is expected to operate between the solute molecules and the bulk phase, which is supported by the plateau appearance of the curves, further[21]. Therefore, specific initial anion concentrations and 10 minutes contact time have been fixed as optimized parameters for forthcoming experimental verification.

**Table 4.4 Impact of Initial Concentration and Agitation Time**

| System | Time (min) | Amount Adsorbed mg/g | | | | | |
|---|---|---|---|---|---|---|---|
| | | 50 mg/L | 100 mg/L | 150 mg/L | 200 mg/L | 250 mg/L | 300 mg/L |
| $PO_4^{3-}$ - TCSS | 5 | 36.42 | 47.38 | 37.65 | 35.84 | 32.74 | 29.62 |
| | 10 | 37.69 | **47.49** | 37.54 | 35.63 | 32.29 | 29.48 |
| | 15 | 36.51 | 47.32 | 36.84 | 35.48 | 31.89 | 29.25 |
| | 20 | 36.72 | 46.54 | 36.62 | 34.53 | 31.56 | 28.94 |
| | 25 | 35.34 | 45.73 | 35.45 | 34.16 | 30.50 | 27.85 |
| | 30 | 35.16 | 44.56 | 35.10 | 33.28 | 30.18 | 27.73 |
| $NO_3^-$ - TCSS | 5 | 36.65 | 46.13 | 42.12 | 39.84 | 37.94 | 34.18 |
| | 10 | 36.43 | **44.14** | 42.65 | 39.55 | 37.67 | 34.15 |
| | 15 | 36.84 | 45.84 | 41.96 | 39.18 | 37.45 | 33.28 |
| | 20 | 36.41 | 44.53 | 41.15 | 38.94 | 36.28 | 33.12 |
| | 25 | 35.90 | 43.14 | 40.84 | 38.38 | 36.14 | 32.24 |
| | 30 | 35.23 | 42.54 | 40.28 | 38.14 | 35.48 | 30.84 |
| $SO_4^{2-}$ - TCSS | 5 | 32.93 | 34.57 | 37.26 | 38.53 | 42.25 | 40.38 |
| | 10 | 33.19 | 34.88 | 37.94 | 39.42 | **46.84** | 41.14 |
| | 15 | 32.58 | 34.28 | 36.74 | 38.25 | 44.32 | 40.89 |
| | 20 | 32.45 | 33.89 | 36.26 | 37.92 | 42.56 | 40.64 |
| | 25 | 32.36 | 33.36 | 35.84 | 37.14 | 41.47 | 39.42 |
| | 30 | 32.14 | 32.68 | 35.56 | 36.67 | 40.79 | 38.93 |

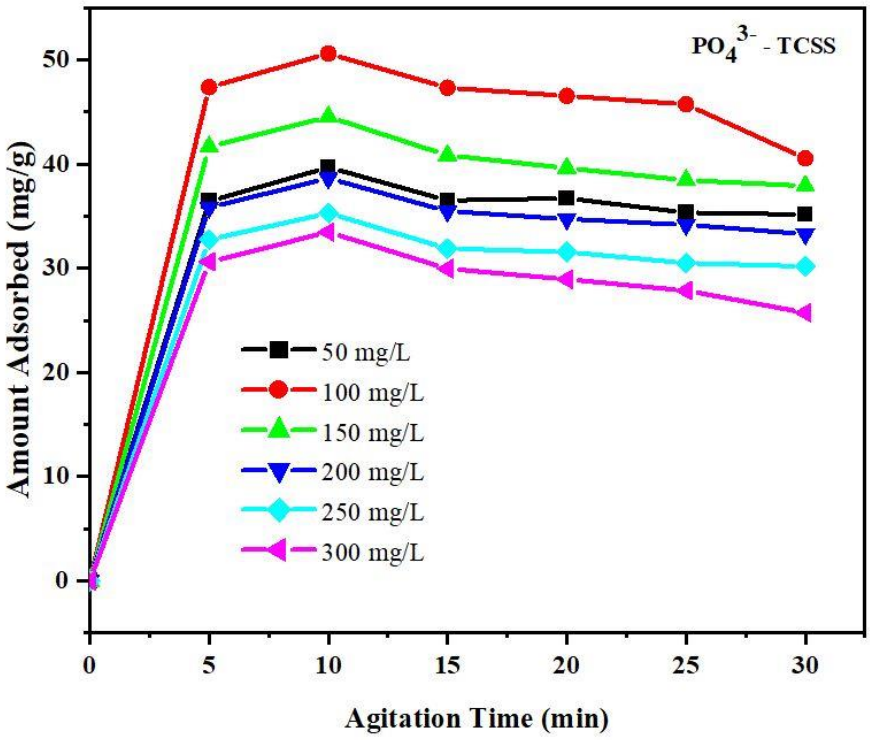


**Figure 4.16 Impact of Initial Concentration and Agitation Time: $PO_4^{3-}$**

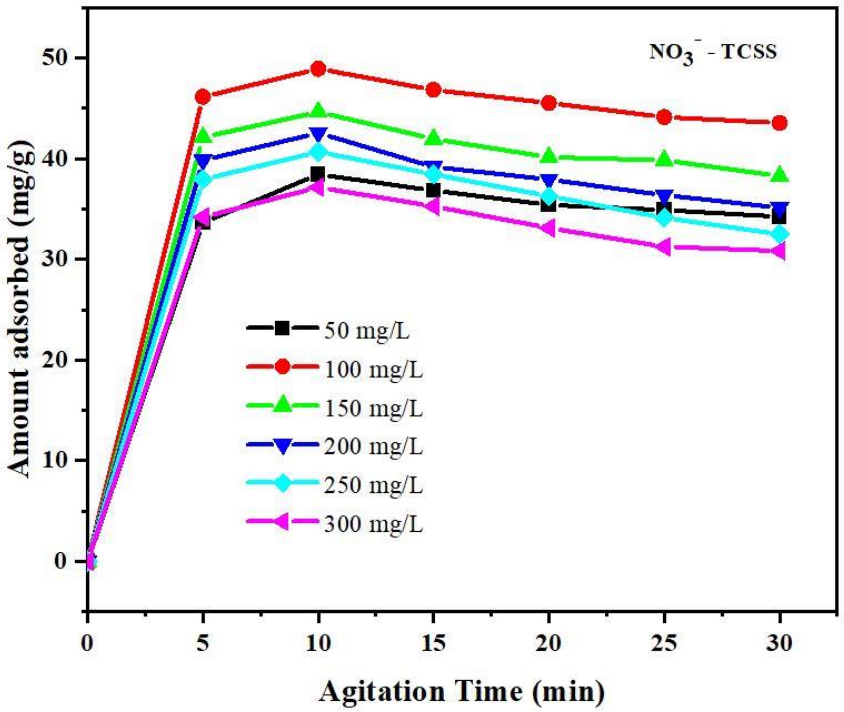


**Figure 4.17 Impact of Initial Concentration and Agitation Time: $NO_3^-$**

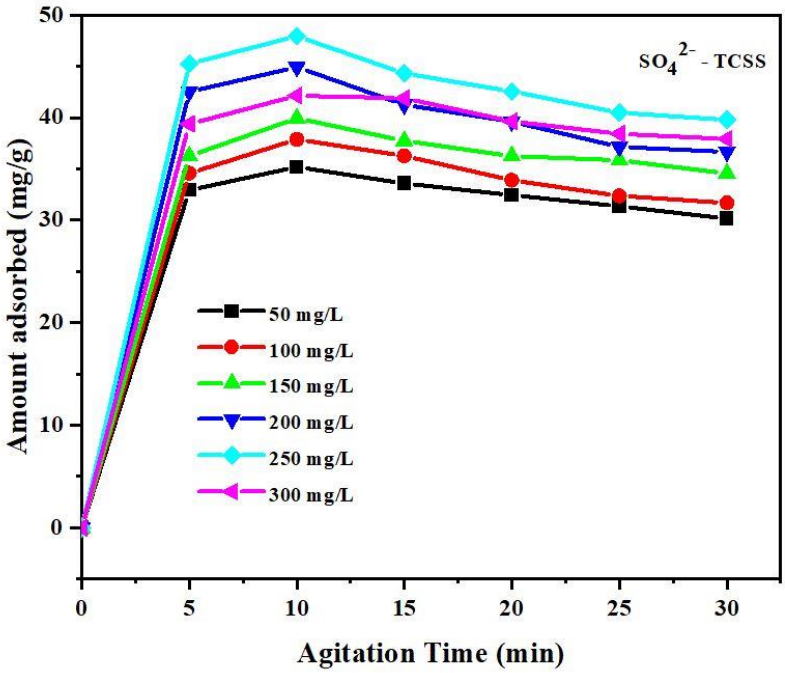


**Figure 4.18 Impact of Initial Concentration and Agitation Time: $SO_4^{2-}$**

### 4.5.3 Impact of Dosage

The impacts of dose variations (50 mg - 300 mg: 50 mg) for the three studied systems are listed in table 4.5. Approximately 95% removal of $PO_4^{3-}$/ $NO_3^-$ and $SO_4^{2-}$ ions is achieved at dosages of 200 and 250 mg respectively. The rate of adsorption was insignificant with further increase in dosage, which shall be due to partial cell aggregation at higher TCSS dose leading to decrease in the number of active sites[22].

**Table 4.5 Impact of Dosage**

| Systems | Percentage removal (%) | | | | | |
|---|---|---|---|---|---|---|
| | **50 mg** | **100 mg** | **150 mg** | **200 mg** | **250 mg** | **300 mg** |
| $PO_4^{3-}$ - TCSS | 89.3 | 93.8 | 94.3 | **95.7** | 93.6 | 89.5 |
| $NO_3^-$ - TCSS | 80.5 | 85.5 | 90.6 | **94.5** | 92.8 | 87.4 |
| $SO_4^{2-}$ - TCSS | 85.4 | 89.4 | 92.9 | 93.82 | **95.3** | 88.3 |

### 4.5.4 Impact of pH

pH value is a key monitoring parameter in sorption technique. Its effect, studied in the range of 3 – 11 is shown in figure 4.19. Maximum anion removal had occurred at pH – 5, may be due to the protonation of TCSS surface at acidic pH promoting strong electrostatic forces of attraction with studied anions, thereby implying positive adsorption[23]. Retarded anion removal at higher pH indicates the competency of hydroxyl ions against studied anions for the sorption sites, leading to lower preferential anion chelation. The above discussions are evidenced from the inverted parabolic curves of the figure. A similar trend has been reported in the removal of anions by Lahieb Faisal Muhaisen et al[24]., and Hakan Demiral et al[25].,.

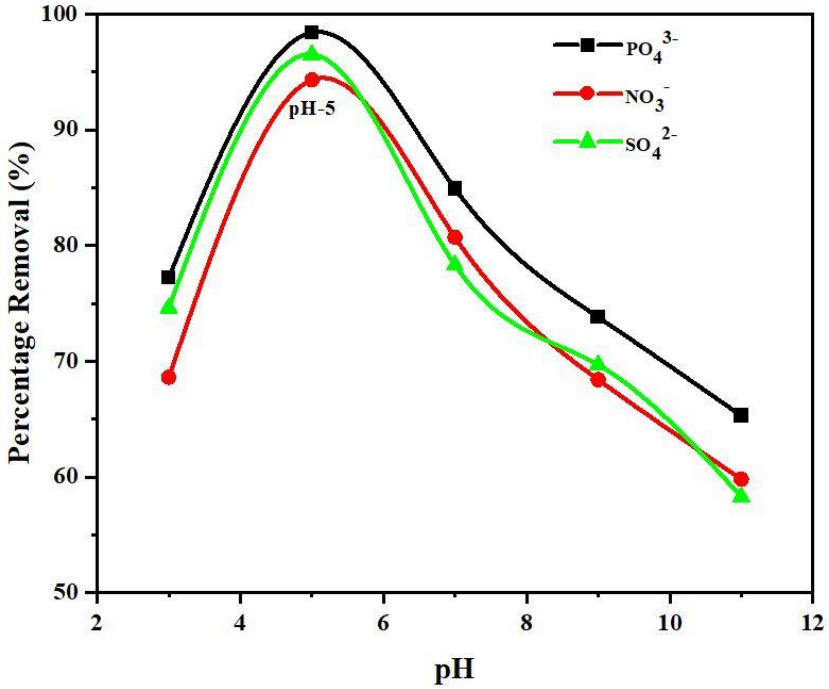


**Figure 4.19 Impact of pH**

### 4.5.5 Impact of Ions

The influence of cations (magnesium and sodium) and anions (chloride and fluoride) on the $PO_4^{3-}$/ $NO_3^-$ / $SO_4^{2-}$ - TCSS systems carried out at varied initial ionic concentrations are listed in table 4.6.

A marked inhibition by $Mg^{2+}$ ion against $Na^{+}$ ion in the percentage removal of the studied anions can be explained by the smaller ionic radii value of $Mg^{2+}$ (0.72 Å) with lesser degree of hydration against greater ionic radii of $Na^{+}$ ion (1.02Å)[26].

$Cl^{-}$ and $F^{-}$ ions exhibited minimal inhibition during adsorption studies. $PO_4^{3-}$ and $SO_4^{2-}$ ions with corresponding three and two valency charges possess greater tendency to get adsorbed, than the monovalent co-ions. Though the studied $NO_3^{-}$ ion and the co-ions are monovalent, the minimal inhibition by the latter is due to their extended hydration energy than the former, with lesser hydration energy, in turn, favouring its adsorption[27].

**Table 4.6 Impact of Ions**

| Systems | Anion removal in absence of ions | Conc. (mg/L) | Percentage Removal (%) | | | |
|---|---|---|---|---|---|---|
| | | | Cations | | Co ions | |
| | | | $Mg^{2+}$ | $Na^{+}$ | $Cl^{-}$ | $F^{-}$ |
| $PO_4^{3-}$ - TCSS | 96.7 | 100 | **76.7** | 78.4 | 86.5 | 89.4 |
| | | 200 | 75.8 | 77.2 | 85.3 | 88.2 |
| | | 300 | 74.3 | 75.8 | 82.7 | 87.4 |
| | | 400 | 70.5 | 73.4 | 81.3 | 86.8 |
| | | 500 | 71.6 | 72.5 | 80.1 | 86.2 |
| $NO_3^{-}$ -TCSS | 94.5 | 100 | **69.3** | 70.2 | 82.8 | 86.3 |
| | | 200 | 68.5 | 69.4 | 81.6 | 85.9 |
| | | 300 | 76.1 | 68.8 | 80.7 | 85.2 |
| | | 400 | 66.5 | 67.3 | 79.3 | 84.6 |
| | | 500 | 64.8 | 66.5 | 78.9 | 83.7 |
| $SO_4^{2-}$ - TCSS | 95.3 | 100 | **74.8** | 75.9 | 84.2 | 88.2 |
| | | 200 | 73.5 | 74.3 | 82.3 | 86.5 |
| | | 300 | 72.8 | 72.6 | 81.6 | 85.3 |
| | | 400 | 70.6 | 70.4 | 80.4 | 84.2 |
| | | 500 | 69.1 | 68.3 | 79.8 | 83.6 |

### 4.5.6 Impact of Temperature

The values (table 4.7) suffice increased anion adsorption with temperatures. The inclined removal might be due to the greater number of active sites on sorbent surface, increased mobility of ions at higher temperatures and reduced boundary layer thickness, reflecting in restriction of mass transfer resistance and surface anion precipitation[28].

**Table 4.7 Impact of Temperature**

| Systems | Percentage Removal (%) | | | | |
|---|---|---|---|---|---|
| | 293 K | 303 K | 313 K | 323 K | 333 K |
| $PO_4^{3-}$ -TCSS | 92.4 | 95.7 | 96.3 | 97.8 | 98.7 |
| $NO_3^-$- TCSS | 91.8 | 94.5 | 95.4 | 96.6 | 97.9 |
| $SO_4^{2-}$ -TCSS | 92.1 | 95.3 | 95.9 | 97.2 | 98.3 |

### 4.6 Desorption/ Regeneration Studies

Notable adsorption capacity and appreciable reusability without significant loss in the sorption ability of modified materials would promote economic value of the method. Desorbing ability of loaded anions and the regenerating capacity of TCSS in consecutive cycles, determined by batch mode studies represented through graph and bar charts respectively (figs 4.20 & 4.21). Increase in concentration of desorbing medium (0.01 – 0.05 N HCl) reflected in the decline of desorption in all the three cases, thus suggesting 0.01N HCl registered a maximum of 93 % recovery[29]. Relationship between regeneration cycles and adsorption capacity of $PO_4^{3-}$ adsorbed by TCSS was maximum viz., 49.53, 47.25 and 45.32 mg/g for the first, second and third cycles and the corresponding desorbed amounts recorded were 36.23, 34.76 and 32.56 mg/g demonstrating regenerating capacity. Similar trends were observed for other two systems, emphasizing the reusability of TCSS.

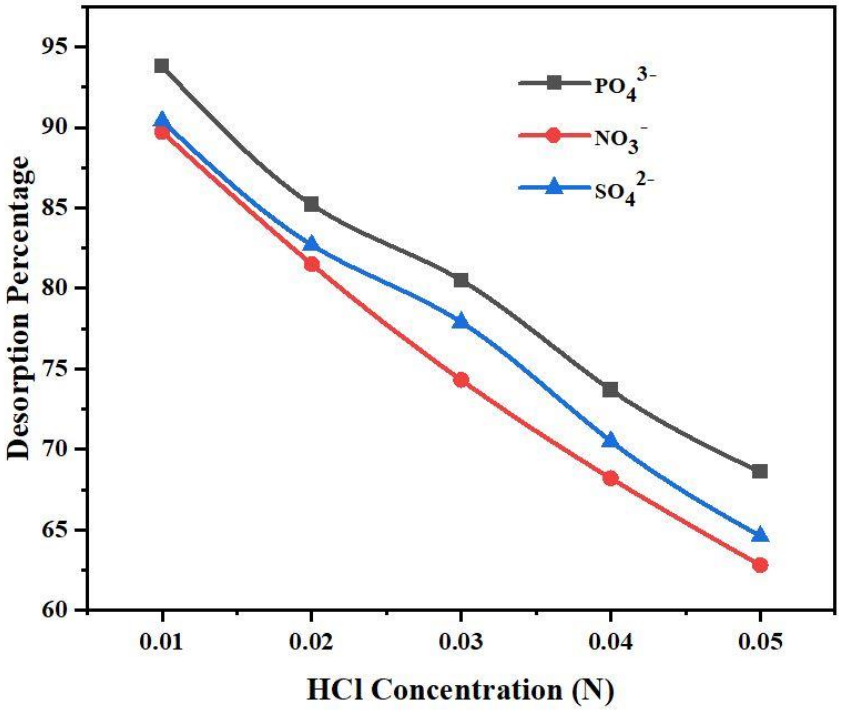


**Figure 4.20 Desorption Plot**

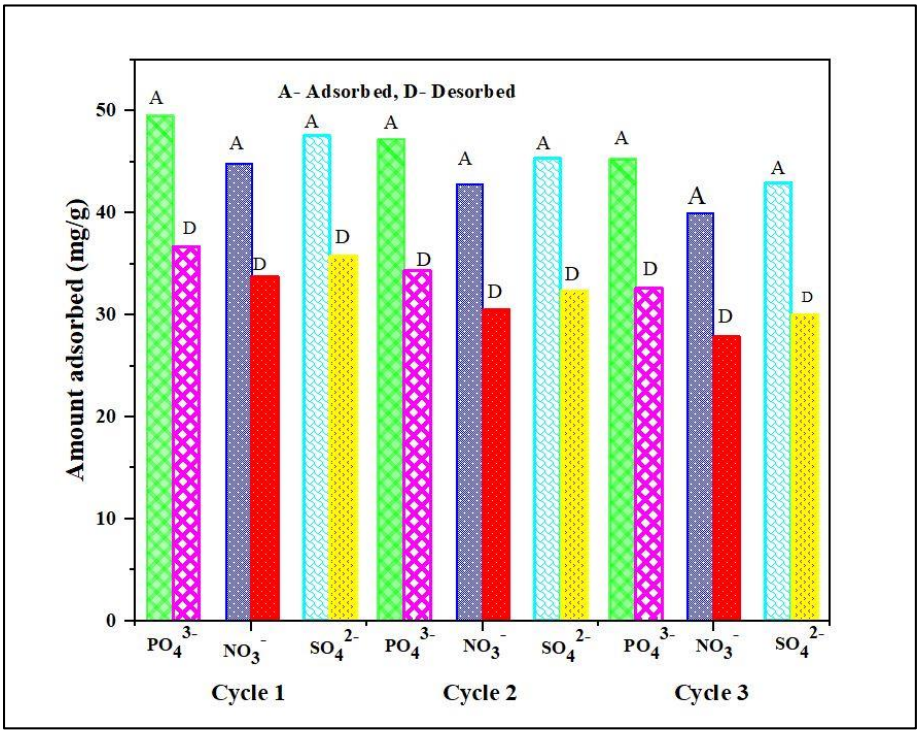


**Figure 4.21 Regeneration Plot**

## 4.7 Statistical Analysis

Batch experimental data determined for TCSS system under their optimized conditions were verified using SPSS 20 software. Descriptive, Correlation and ANOVA studies to assess the significant level of particle size, anion concentration, dosage and pH were statistically calculated and recorded in table 4.8.

Negative Pearson co-efficient values in most parameters favour extended sorption. Probability (P) values observed to be less than the significant value implies rejection of null hypothesis for all the studied anions[30]. $F > F_{crit}$ values derived from ANOVA calculations fulfil statistical significance.

**Table 4.8 Statistical Data**

| System | Parameter | Descriptive | | | Pearson Correlation | p | ANOVA | |
|---|---|---|---|---|---|---|---|---|
| | | Mean | SD | SE | | | F | $F_{crit}$ |
| $PO_4^{3-}$ - TCSS | Particle size | 37.96 | 8.07 | 3.61 | -0.9182 | $6.31E^{-06}$ | 108.26 | 5.31 |
| | Initial anion concentration | 36.93 | 6.69 | 2.73 | -0.7418 | 0.0047 | 13.00 | 4.96 |
| | Dosage | 39.50 | 6.95 | 2.83 | 0.5036 | 0.0053 | 12.51 | 4.96 |
| | pH | 41.66 | 5.48 | 2.45 | -0.6042 | $1.85E^{-06}$ | 149.68 | 5.31 |
| $NO_3^-$- TCSS | Particle size | 39.26 | 6.94 | 3.10 | -0.9698 | $1.5E^{-06}$ | 156.66 | 5.31 |
| | Initial anion concentration | 39.47 | 4.45 | 1.81 | -0.4890 | 0.0053 | 12.56 | 4.96 |
| | Dosage | 38.42 | 6.76 | 2.76 | 0.5122 | 0.0051 | 12.72 | 4.96 |
| | pH | 40.62 | 4.71 | 2.10 | -0.7847 | $1.01E^{-06}$ | 175.26 | 5.31 |
| $SO_4^{2-}$ TCSS | Particle size | 36.86 | 7.60 | 3.40 | -0.9026 | $5.01E^{-06}$ | 115.10 | 5.31 |
| | Initial anion concentration | 39.05 | 5.16 | 2.10 | 0.8269 | 0.0052 | 12.63 | 4.96 |
| | Dosage | 36.51 | 6.89 | 2.81 | 0.6494 | 0.0047 | 13.08 | 4.96 |
| | pH | 40.66 | 5.14 | 2.30 | -0.5449 | $1.61E^{-06}$ | 155.18 | 5.31 |

## 4.8 Adsorption Isotherms

Adsorption process is well understood through isotherm models which describe the relation between adsorbate concentration with respect to amount of sorbate adsorbed per unit mass of sorbent[31]. Experimentally verified data as applied to the isothermal equations, listed in table 4.9, were fitted into Langmuir (fig 4.22), Freundlich (fig 4.23), Temkin (fig 4.24) and Dubinin – Radushkevich (fig 4.25) isotherm plots. Isothermal constants deduced from the slopes and intercepts of the linear graphs, the correlation coefficients ($R^2$) and mean free energy (E) are summarized in table 4.10.

**Table 4.9 Equilibrium Concentrations- Isothermal Study**

| System | Anion Conc. (mg/L) | Langmuir | | Freundlich | | Temkin | | DKR | |
|---|---|---|---|---|---|---|---|---|---|
| | | $C_e$ | $C_e/q_e$ | log $C_e$ | log $q_e$ | ln $C_e$ | $q_e$ | E*$10^{-5}$ | ln $q_e$ |
| $PO_4^{3-}$ - TCSS | 50 | 1.82 | 0.19 | 0.26 | 0.96 | 0.59 | 1.18 | 12.16 | 2.21 |
| | 100 | 5.13 | 0.26 | 0.71 | 1.28 | 1.63 | 1.36 | 2.01 | 2.96 |
| | 150 | 7.42 | 0.30 | 0.87 | 1.38 | 2.24 | 1.52 | 1.01 | 3.19 |
| | 200 | 13.89 | 0.41 | 1.14 | 1.52 | 2.76 | 1.60 | 0.30 | 3.51 |
| | 250 | 24.55 | 0.61 | 1.39 | 1.59 | 3.20 | 1.72 | 0.10 | 3.68 |
| | 300 | 43.62 | 0.97 | 1.63 | 1.65 | 3.77 | 1.67 | 0.03 | 3.79 |
| $NO_3^-$ - TCSS | 50 | 1.13 | 0.07 | 0.05 | 1.99 | 0.12 | 1.53 | 25.50 | 2.74 |
| | 100 | 3.99 | 0.18 | 0.60 | 1.33 | 1.38 | 1.62 | 3.17 | 3.07 |
| | 150 | 5.59 | 0.20 | 0.74 | 1.44 | 1.72 | 1.69 | 1.71 | 3.32 |
| | 200 | 9.36 | 0.29 | 0.97 | 1.50 | 2.23 | 1.73 | 0.65 | 3.45 |
| | 250 | 23.14 | 0.64 | 1.36 | 1.55 | 3.14 | 1.79 | 0.11 | 3.57 |
| | 300 | 39.17 | 1.00 | 1.59 | 1.58 | 3.66 | 1.82 | 0.04 | 3.65 |
| $SO_4^{2-}$ TCSS | 50 | 1.63 | 0.07 | 0.21 | 1.31 | 0.48 | 1.42 | 14.52 | 3.01 |
| | 100 | 3.54 | 0.12 | 0.54 | 1.45 | 1.26 | 1.48 | 3.92 | 3.34 |
| | 150 | 7.24 | 0.19 | 0.85 | 1.57 | 1.97 | 1.53 | 1.06 | 3.62 |
| | 200 | 13.13 | 0.33 | 0.11 | 1.59 | 2.57 | 1.57 | 0.34 | 3.67 |
| | 250 | 18.23 | 0.44 | 1.26 | 1.60 | 2.90 | 1.64 | 0.18 | 3.70 |
| | 300 | 24.94 | 0.57 | 1.39 | 1.64 | 3.21 | 1.67 | 0.09 | 3.77 |

**Table 4.10 Isothermal Constants**

| Systems | Langmuir Isotherm | | | Freundlich Isotherm | | | Temkin Isotherm | | | DKR Isotherm | | |
|---|---|---|---|---|---|---|---|---|---|---|---|---|
| | $q_m$ (mg/g) | b | $R^2$ | $K_F$ (mg/g) | 1/n | $R^2$ | $A_T$ (L/g) | $B_T$ (J/mol) | $R^2$ | $q_s$ (mg/g) | E (KJ/mol) | $R^2$ |
| $PO_4^{3-}$ - TCSS | **54.70** | 0.14 | 0.9997 | 7.99 | 2.00 | 0.9791 | 0.12 | 198.85 | 0.9486 | 33.90 | 2.10 | 0.8437 |
| $NO_3^-$- TCSS | **44.16** | 0.32 | 0.9980 | 15.92 | 3.80 | 0.9648 | 0.24 | 370.81 | 0.9292 | 31.79 | 4.10 | 0.7475 |
| $SO_4^{2-}$ TCSS | **49.74** | 0.46 | 0.9983 | 19.49 | 3.73 | 0.9694 | 0.29 | 303.32 | 0.9305 | 40.01 | 3.19 | 0.9222 |

### 4.8.1 Langmuir Model

Langmuir constant ($q_m$) interpreting sorption capacity as 51.72 mg/g, 43.16 mg/g, 46.74 mg/g for $PO_4^{3-}$, $NO_3^-$, $SO_4^{2-}$ respectively, exhibit good agreement with adsorption capacities as per batch studies. $R^2$ values calculated for the Langmuir plot is almost near to unity favouring the fit in of the Langmuir model for all the systems[32]. Equilibrium parameter values ($R_L$), a dimensionless separation factor, calculated from the sorption intensity (b) is listed in table 4.11. These values fall in within 0 - 1 reveal favourable adsorption for Langmuir model.

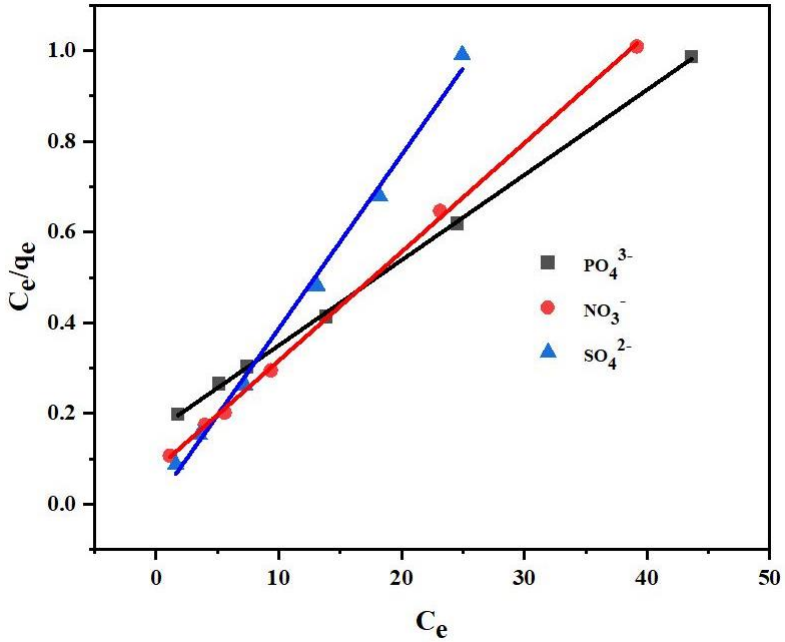


**Figure 4.22 Langmuir Plot**

**Table 4.11 Equilibrium Parameter ($R_L$)**

| Conc. mg/L | $PO_4^{3-}$ - TCSS | $NO_3^-$-TCSS | $SO_4^{2-}$ TCSS |
|---|---|---|---|
| 50 | 0.12 | 0.05 | 0.04 |
| 100 | 0.06 | 0.03 | 0.02 |
| 150 | 0.04 | 0.02 | 0.01 |
| 200 | 0.03 | 0.01 | 0.01 |
| 250 | 0.02 | 0.01 | 0.08 |
| 300 | 0.02 | 0.01 | 0.07 |

### 4.8.2 Freundlich Model

Freundlich isotherm is commonly used to study sorption occurring on heterogeneous surfaces. 1/n value indicates the degree of non-linearity between solution concentration and sorbent material. Generally, if 1/n value is lower than 1, the sorption process is understood to be more of chemical nature[33]. However, the calculated values of 1/n being greater than 1 for the TCSS systems, indicate the nature of sorption to be physical.

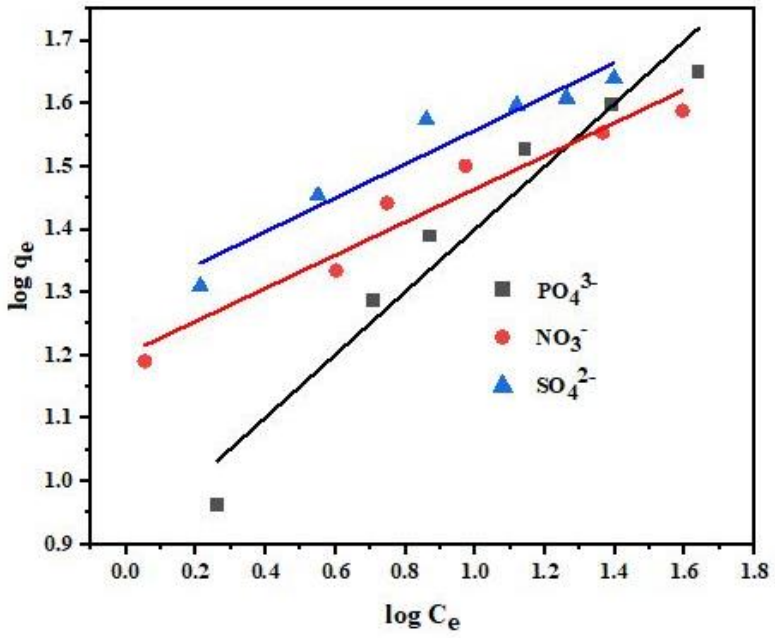


**Figure 4.23 Freundlich Plot**

### 4.8.3 Temkin Isotherm Model

Lower $A_T$ (binding constant) and higher $B_T$ (heat of adsorption) values arrived from Temkin plot represent weak sorbate/ sorbent interactions[34]. This is made from the observations of improper fit of linearity due to scattered points of $q_e$ and ln $C_e$ values. Further, correlation coefficient values (≈ 0.9000) favour least applicability of Temkin model for the reported systems.

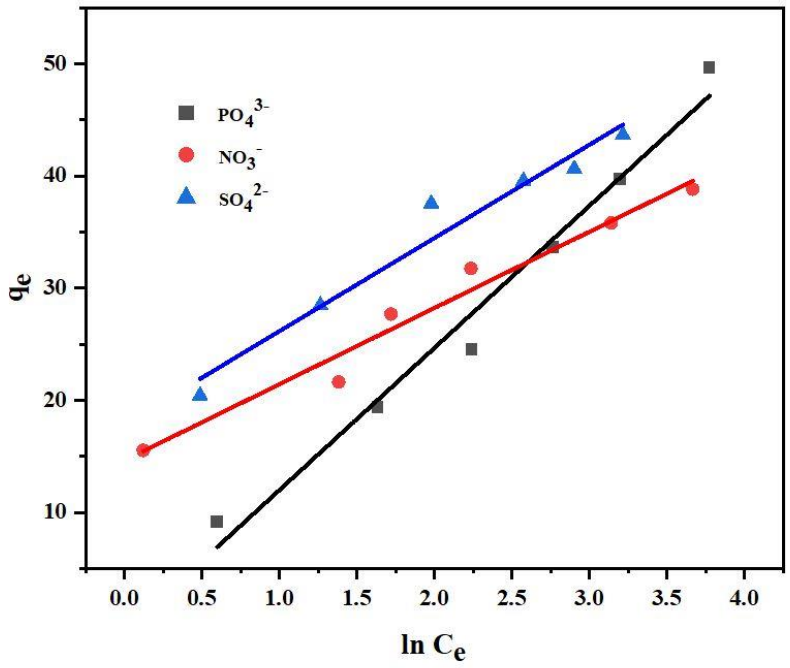


**Figure 4.24 Temkin Plot**

### 4.8.4 Dubinin–Kaganer-Radushkevich (DKR) Model

DKR isotherm is applied to estimate the mean free energy in process of determining sorption nature of the system. Mean free energy (E) values calculated as per equation 16 (in chapter III under 3.26.4) using βDR constant value are observed to be 2.10, 4.10 and 3.19 KJ/ mol for $PO_4^{3-}$, $NO_3^-$ and $SO_4^{2-}$ sorption. These values less than 8 KJ/ mol reveal that the systems are favoured by monolayer coverage[36].

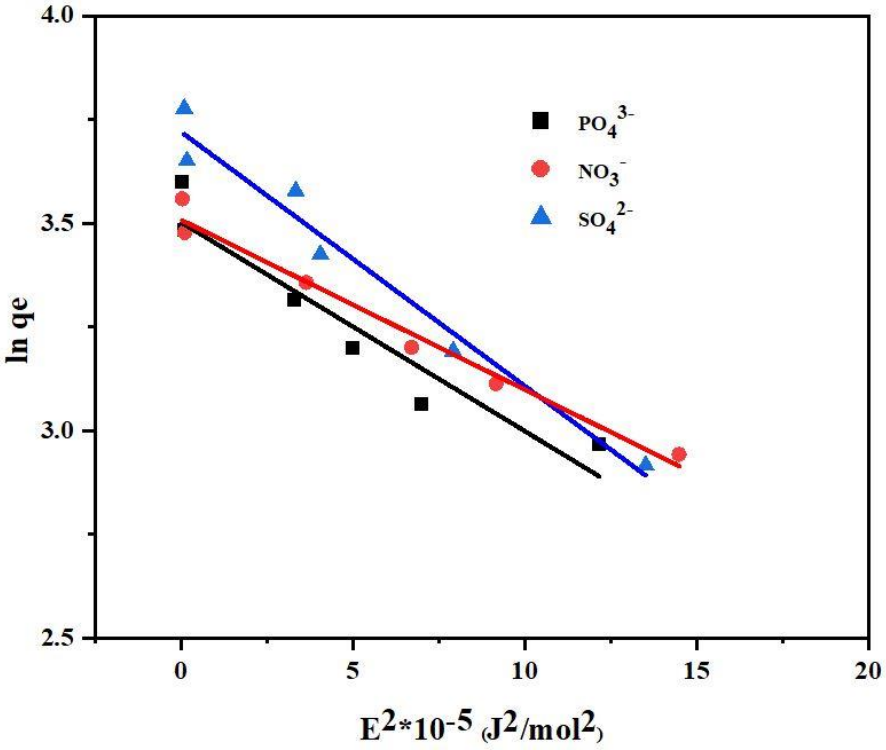


**Figure 4.25 DKR Plot**

### 4.8.5 Comparison of Isotherm Models

Experimental data, as resulted from optimized conditions, recorded 49.26 mg/g, 46.92 mg/g and 47.95 mg/g for $PO_4^{3-}$/ $NO_3^-$ and $SO_4^{2-}$ systems, which are in good agreement with the calculated isothermal constant values ($q_m$ - 51.72 mg/g, 43.16 mg/g, 46.74 mg/g) referring, the adsorption capacity to be in lieu of Langmuir model. This is further supported by $R^2$ values, nearness to unity, as evident from the linearity of Langmuir plots. Since, isothermal constants for other models do not validate the batch output, the studied systems follow monolayer adsorption, favouring the applicability of Langmuir isothermal model.

## 4.9 Adsorption Kinetics

Kinetic studies play a key role in describing the adsorption mechanism, mass transfer process and potentiality of rate controlling step during the sorption process[37]. Pertinence of Pseudo first order, Pseudo second order, Elovich and Intra particle diffusion

models were studied using calculated experimental data as per table 4.12. Equilibrium adsorption capacities ($q_{cal}$), Pseudo model constants ($K_1$, $K_2$), Correlation coefficients ($R^2$), sum of squares of error (SSE) values calculated from the respective plots (figs 4.26, 4.27), with reference to the observed experimental data for the three systems are listed in table 4.13.

**Table 4.12 Pseudo Models – Data**

| Time (t) (min) | $PO_4^{3-}$ - TCSS ($q_e$ -100 mg/L) | | | $NO_3^-$ - TCSS ($q_e$ -100 mg/L) | | | $SO_4^{2-}$ - TCSS ($q_e$ -250 mg/L) | | |
|---|---|---|---|---|---|---|---|---|---|
| | Log ($q_e$-$q_t$) | $q_t$ | $t/q_t$ | Log ($q_e$-$q_t$) | $q_t$ | $t/q_t$ | Log ($q_e$-$q_t$) | $q_t$ | $t/q_t$ |
| 5 | 1.92 | 15.32 | 0.19 | 1.90 | 13.87 | 0.36 | 2.35 | 23.86 | 0.20 |
| 10 | 1.91 | 18.16 | 0.42 | 1.91 | 14.69 | 0,68 | 2.35 | 35.67 | 0.38 |
| 15 | 1.89 | 20.83 | 0.67 | 1.91 | 16.25 | 0.92 | 2.34 | 26.34 | 0.56 |
| 20 | 1.89 | 22.17 | 0.96 | 1.92 | 18.34 | 1.09 | 2.34 | 28.40 | 0.70 |
| 25 | 1.88 | 23.64 | 1.37 | 1.93 | 19.22 | 1.30 | 2.34 | 30.13 | 0.82 |
| 30 | 1.87 | 25.59 | 1.95 | 1.93 | 20.46 | 1.46 | 2.33 | 32.45 | 0.92 |

### 4.9.1 Pseudo First Order Model

Pseudo first order plot (log $q_e$-$q_t$ vs t) as depicted in figure 4.26, reveal lower correlation coefficient values (< 0.90) and marked variations in the calculated sorption capacity ($q_{cal}$) values from the graph against that registered in the experimental data ($q_{exp}$). These observations imply the unfavourable condition of applying Pseudo-first order model for the systems. This is further supported by higher SSE values which does not favour positive adsorption.

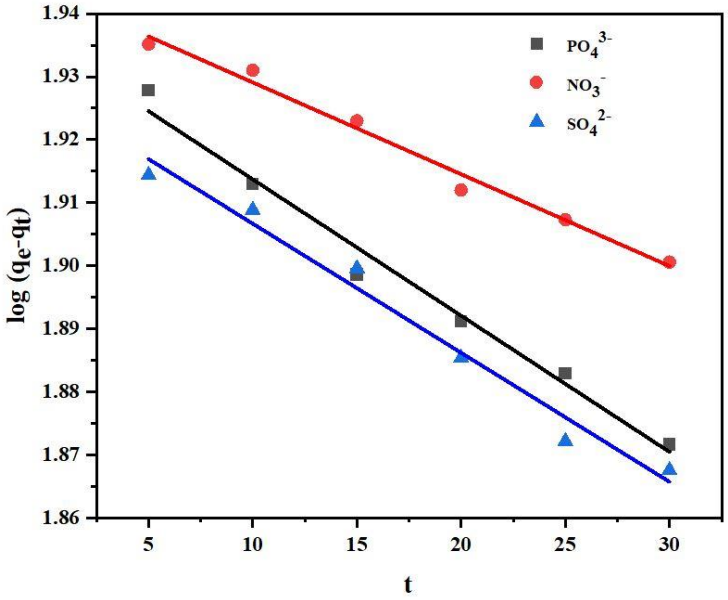


**Figure 4.26 Pseudo First Order Model**

### 4.9.2 Pseudo Second Order Model

Plot of $t/q_t$ versus t (fig 4.27) shows $R^2$ values near to unity, as derived from the straight lines. Also, the $q_{cal}$ values (antilog of intercept) in lieu with $q_{exp}$ values favour the suitability of pseudo-second-order model to describe the adsorption kinetics, being sufficed with minimal SSE values[38].

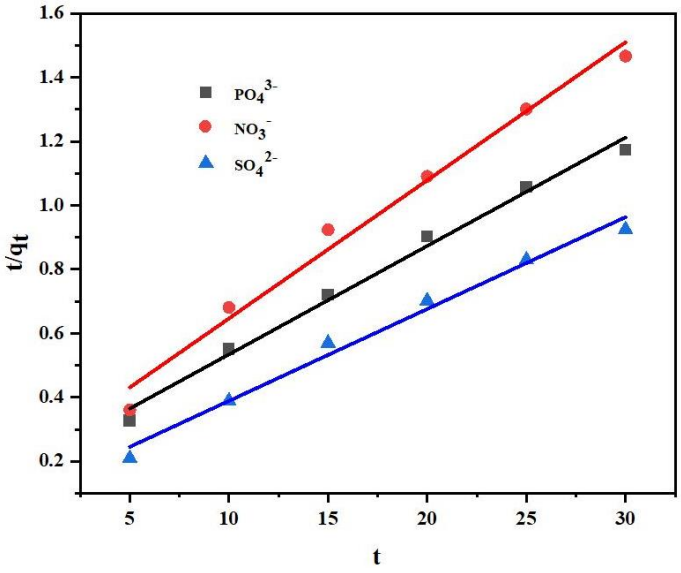


**Figure 4.27 Pseudo Second Order Model**

**Table 4.13 Pseudo First Order/ Pseudo Second Order Parametric values**

| Conc. of Anions (mg/L) | $q_{exp}$ (mg/g) | Pseudo First Order | | | | Pseudo Second Order | | | |
|---|---|---|---|---|---|---|---|---|---|
| | | $q_{cal}$ (mg/g) | $K_1 \times 10^{-3}$ ($min^{-1}$) | $R^2$ | SSE | $q_{cal}$ (mg/g) | $K_2 \times 10^{-3}$ ($min^{-1}$) | $R^2$ | SSE |
| **$PO_4^{3-}$ - TCSS** | | | | | | | | | |
| 50 | 37.69 | 17.37 | 0.53 | 0.8886 | 3.17 | 35.71 | 0.46 | 0.9997 | 0.11 |
| 100 | **57.26** | 86.15 | 0.50 | 0.8933 | 6.46 | **47.49** | 0.58 | 0.9908 | 2.98 |
| 150 | 37.54 | 120.06 | 0.92 | 0.8945 | 13.73 | 36.33 | 0.42 | 0.9997 | 0.22 |
| 200 | 35.63 | 173.22 | 0.69 | 0.8380 | 22.89 | 33.15 | 0.32 | 0.9994 | 0.78 |
| 250 | 32.29 | 226.04 | 0.46 | 0.8478 | 32.21 | 30.01 | 0.34 | 0.9994 | 0.45 |
| 300 | 29.48 | 279.12 | 0.46 | 0.8262 | 41.58 | 27.77 | 0.27 | 0.9989 | 0.47 |
| **$NO_3^-$ - TCSS** | | | | | | | | | |
| 50 | 32.43 | 23.12 | 0.62 | 0.8632 | 1.55 | 31.44 | 0.32 | 0.9997 | 0.16 |
| 100 | **48.92** | 87.84 | 0.34 | 0.8659 | 6.82 | **44.14** | 2.02 | 0.9956 | 3.96 |
| 150 | 40.65 | 125.48 | 0.92 | 0.8862 | 14.13 | 38.49 | 0.34 | 0.9989 | 2.02 |
| 200 | 37.55 | 177.13 | 0.69 | 0.8338 | 23.26 | 36.38 | 0.39 | 0.9994 | 1.86 |
| 250 | 35.67 | 229.72 | 0.46 | 0.8936 | 32.34 | 34.33 | 0.36 | 0.9996 | 1.89 |
| 300 | 33.15 | 284.11 | 0.69 | 0.8767 | 41.82 | 32.17 | 0.18 | 0.9956 | 1.83 |
| **$SO_4^{2-}$ - TCSS** | | | | | | | | | |
| 50 | 33.19 | 30.81 | 0.73 | 0.8469 | 1.11 | 31.52 | 0.17 | 0.9978 | 0.39 |
| 100 | 34.88 | 73.06 | 018 | 0.8316 | 6.36 | 32.72 | 0.19 | 0.9973 | 2.02 |
| 150 | 37.74 | 125.95 | 0.13 | 0.8431 | 14.66 | 35.85 | 0.22 | 0.9986 | 1.34 |
| 200 | 39.42 | 174.22 | 0.92 | 0.8284 | 22.46 | 37.94 | 0.21 | 0.9989 | 1.24 |
| 250 | **52.95** | 228.08 | 0.16 | 0.8516 | 30.52 | **46.84** | 0.81 | 0.9966 | 2.40 |
| 300 | 41.14 | 276.18 | 0.69 | 0.8196 | 39.17 | 40.48 | 0.18 | 0.9963 | 1.77 |

### 4.9.3 Elovich Model

Homogenous / heterogenous nature of any solid surface possessing sorption characteristics in favour of its adsorption pattern is well explained by Elovich model[39]. Kinetic rate constants: initial adsorption rate (α); extent of surface coverage (β) derived from the intercepts and slopes of Elovich plot, (fig 4.28), along with $R^2$ values are shown in table 4.14. It is inferred from the table, that the constants α and β are inversely related at all the studied concentrations of the anions. A study increases in the β values with respect to increasing concentrations shall be due to extensive surface coverage onto TCSS, leading to increased activation energy[40]. Non linearity of the plotted points with lesser $R^2$ values imply less favourable nature of Elovich model to be applied to the studied systems.

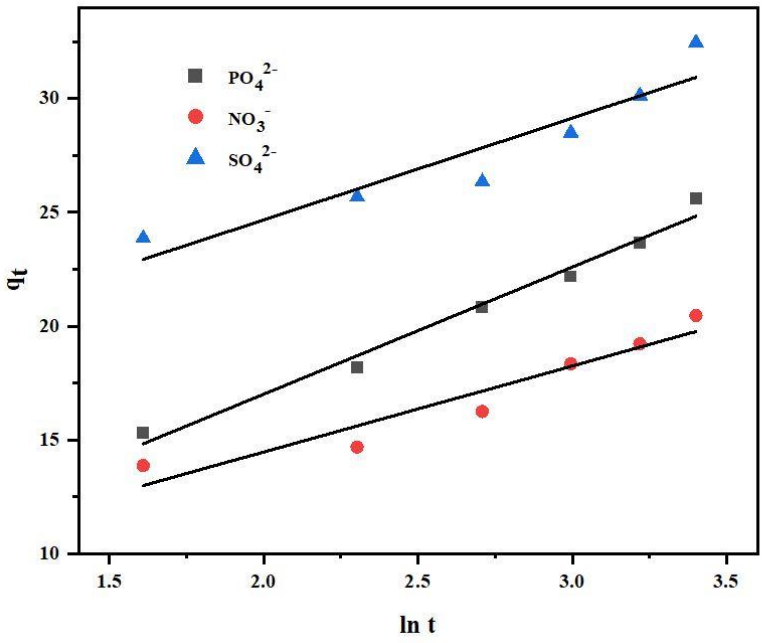


**Figure 4.28 Elovich Plot**

**Table 4.14 Elovich Constants**

| Conc. (mg/L) | $PO_4^{3-}$ - TCSS | | | $NO_3^-$ - TCSS | | | $SO_4^{2-}$ - TCSS | | |
|---|---|---|---|---|---|---|---|---|---|
| | **α** | **β** | **$R^2$** | **α** | **β** | **$R^2$** | **α** | **β** | **$R^2$** |
| 50 | 31.02 | 1.16 | 0.8328 | 29.11 | 1.44 | 0.8268 | 22.26 | 1.48 | 0.8188 |
| 100 | 28.91 | 1.27 | 0.8943 | 26.91 | 1.57 | 0.8843 | 21.59 | 1.77 | 0.8507 |
| 150 | 26.90 | 1.38 | 0.8254 | 22.38 | 1.78 | 0.8530 | 20.26 | 1.93 | 0.8453 |
| 200 | 24.19 | 1.65 | 0.8106 | 20.72 | 1.84 | 0.8727 | 18.59 | 2.16 | 0.8230 |
| 250 | 21.51 | 1.75 | 0.8388 | 17.59 | 2.07 | 0.8357 | 17.25 | 2.79 | 0.8957 |
| 300 | 17.93 | 1.98 | 0.8400 | 12.68 | 2.27 | 0.8682 | 15.74 | 2.98 | 0.8369 |

### 4.9.4 Intraparticle Diffusion Model

Two portions (inclined, steep) as obvious from the plot (fig 4.29) indicate that sorption had occurred on the sorbent's surface followed by intraparticle diffusion[41]. Values of boundary layer thickness (C) and pore diffusion ($K_{id}$) related to the first and second parts of the curves were calculated from the intercepts and slopes respectively and listed in table 4.15. The contribution of interior sorption sites of TCSS is significant with larger diffusion rate in the attainment of saturation point.[42] $K_{id}$ values being directly proportional to initial anion concentrations reveal extended diffusion for increased sorbate species. Amongst the three anions, marked $K_{id}$ values is observed for phosphate ion, for which the reason could be better diffusive nature with respect to ionic valency.

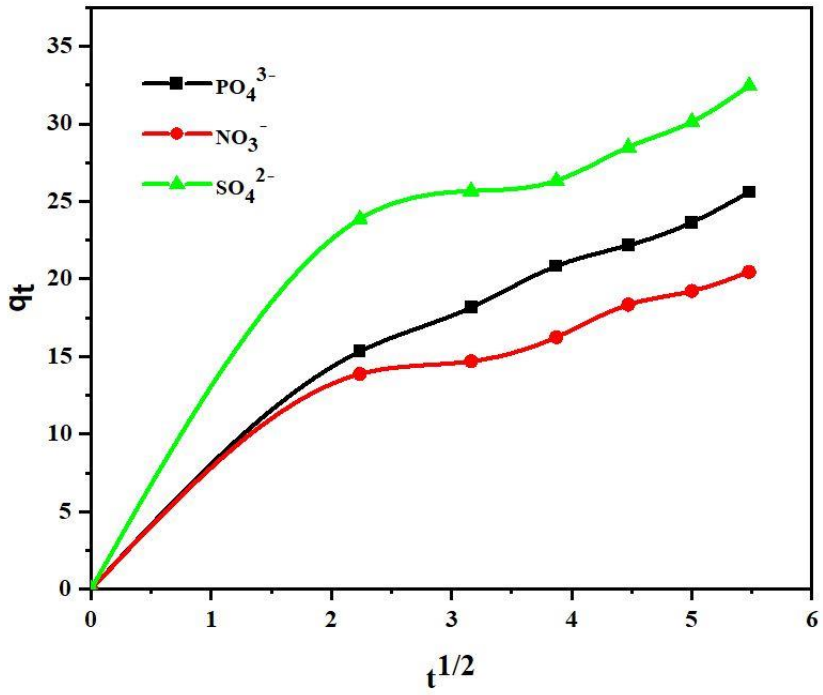


**Figure 4.29 Intraparticle Diffusion Plot**

**Table 4.15 Intraparticle Diffusion Constants**

| Conc. (mg/L) | $PO_4^{3-}$ - TCSS | | $NO_3^-$- TCSS | | $SO_4^{2-}$ - TCSS | |
|---|---|---|---|---|---|---|
| | $K_{id}$ | C | $K_{id}$ | C | $K_{id}$ | C |
| 50 | 1.65 | 22.51 | 1.04 | 25.03 | 1.56 | 16.54 |
| 100 | 2.55 | 25.48 | 1.54 | 28.48 | 2.14 | 17.52 |
| 150 | 2.86 | 28.55 | 1.86 | 32.99 | 2.76 | 21.82 |
| 200 | 3.37 | 35.01 | 2.38 | 41.40 | 2.97 | 23.32 |
| 250 | 3.69 | 38.30 | 2.95 | 48.51 | 3.51 | 26.32 |
| 300 | 3.80 | 44.85 | 3.29 | 53.60 | 3.78 | 31.30 |

### 4.9.5 Comparison of Kinetic Models

Pseudo-second-order model with $R^2$ values almost near to one, suggested the notable linearity of the plot in preference to Pseudo-first-order and Elovich models, where their $R^2$ values are in the range of 0.8100 – 0.8900 only. This statement in favour of Pseudo-second-order model, is supported by the obtained $q_{cal}$ values, more similar to the numericals of the amount adsorbed as per experimental observations.

## 4.10 Adsorption Dynamics

Thermodynamic constants ΔG°, ΔH° and ΔS° are derived from the slopes and intercepts of Van't Hoff's plot (ln $K_C$ vs 1/T) as depicted in figure 4.30. Change in free energy with respect to different temperatures at which the sorption systems were experimentally verified, are calculated as per equation 22 (in chapter III under 3.16). Negative values of ΔG° and positive values of ΔH°/ΔS° (table 4.16) imply the feasibility/spontaneity, endothermicity/extended mobility at the solid/liquid interfaces during the reaction. Similar trend was recorded by authors while studying the sorption characteristics of soya bean husk, red mud and rice straw[42,43,44].

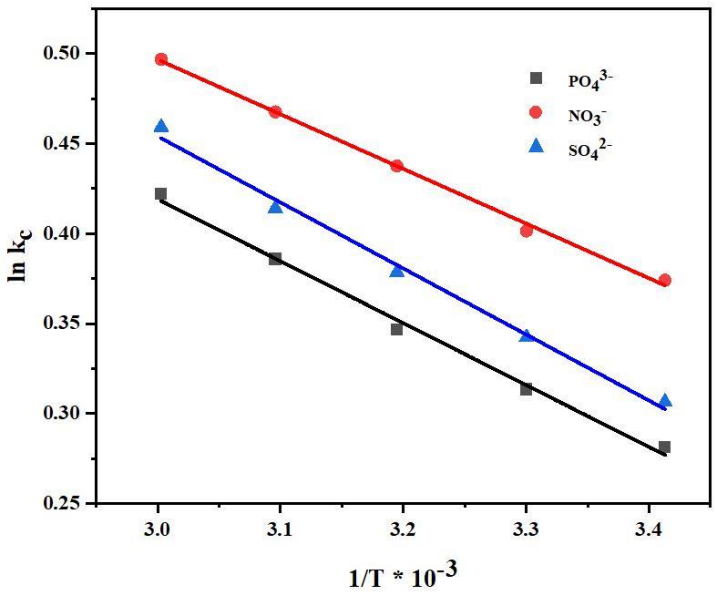


**Figure 4.30 Van't Hoff's Plot**

**Table 4.16 Thermodynamic Constants**

| Temp. (K) | $PO_4^{3-}$ - TCSS | | | $NO_3^-$ - TCSS | | | $SO_4^{2-}$ - TCSS | | |
|---|---|---|---|---|---|---|---|---|---|
| | $\Delta G° \times 10^{-3}$ kJ/ mol | $\Delta H°$ kJ/ mol | $\Delta S°$ kJ/ mol | $\Delta G° \times 10^{-3}$ kJ/ mol | $\Delta H°$ kJ/ mol | $\Delta S°$ kJ/ mol | $\Delta G° \times 10^{-3}$ kJ/ mol | $\Delta H°$ kJ/ mol | $\Delta S°$ kJ/ mol |
| 293 | -0.68 | 2.86 | 12.07 | -0.91 | 2.52 | 11.70 | -0.74 | 3.05 | 12.92 |
| 303 | -0.78 | | | -1.01 | | | -0.86 | | |
| 313 | -0.90 | | | -1.13 | | | -0.98 | | |
| 323 | -1.03 | | | -1.25 | | | -1.11 | | |
| 333 | -1.16 | | | -1.37 | | | -1.27 | | |

## 4.11 References


[1] S.R. Sugunadevi, M.Sathishkumar, K.Shanthi, K.Kadirvelu, S.Pattabhi, Removal of Direct T-blue R from aqueous solution onto carbonised sugarcane baggase waste, *Indian J. Environ. Protection*. 22 **(2002)** 500-505

[2] IUPAC Manual of Symbols and Terminology of Colloid Surface, Butterworths, London, **(1982)**.

[3] V. C. Srivastava, I. D. Mall and I. M. Mishra, Characterization of Mesoporous Rice Husk Ash (RHA) and Adsorption Kinetics of Metal Ions from Aqueous Solution onto RHA, *Journal of Hazardous Materials*, 134 **(2006)** 257-267

[4] Katsumi Kaneko, Determination of pore size distribution -Adsorbents and catalysts, *Journal of Membrane Science*, 96 **(1994)** 59-89

[5] C Liu, Hu Ngo, W Guo, KL Tung, Optimal conditions for preparation of banana peels, sugarcane bagasse and watermelon rind in removing copper from water, *Bioresource Technology*, 119 **(2012)** 349-354

[6] M. K. Mondal, Removal of Pb (II) from Aqueous Solution by Adsorption using Activated Tea Waste, *Korean Journal of Chemical Engineering*, 27 (1) **(2012)** 144–151

[7] D. H. K. Reddy, D. K. V. Ramana and A. V. R. Seshaiah Reddy Biosorption of Ni (II) from Aqueous Phase by Moringa Oleifera Bark, a Low Cost Biosorbent. *Desalination*, 268 **(2011)** 150–157

[8] Roozbeh Hoseinzadeh Hesas, Arash Arami- Niya, Wan Mohd Ashri Wan Daud, Preparation and characterisation of Activated carbon from Apple waste by microwave assisted phosphoric acid activation: Application in Methylene blue adsorption, *BioResources*, 8(2) **(2013)** 2950-2966

[9] F. Taner, I. Ardic, B. Halisdemir and E Pehlivan, Biomass use and Potential in Turkey. In: Biomass and Agricultural: Sustainability, *Markets and Policies. OED publication* **(2004)**

[10] Chunhui Fana, Yingchao Zhang, Adsorption isotherms, kinetics and thermodynamics of nitrate and phosphate in binary systems on a novel adsorbent derived from corn stalks, *Journal of Geochemical Exploration,* 188 **(2019)** 95 -100

[11] Lin Wang, Zhizhi Xu, Yongsheng Fu, Yangwu Chen, Zhicheng Pan, Rui Wanga and Zhouliang Tan, Comparative analysis on adsorption properties and mechanisms of nitrate and phosphate by modified corn stalks, *Royal Society of Chemistry Advances,* 8 **(2018)** 38468 – 36476

[12] Tarun Kumar Naiya, Pankaj Chowdhury, Ashim Kumar Bhattacharya, Sudip Kumar Das, Sawdust and Neem Bark as Low-Cost Natural Biosorbent for Adsorptive Removal of Zn (II) and Cd (II) Ions from Aqueous solutions, *Chemical Engineering Journal*, 148 **(2009)** 68-79

[13] Ahmet Ornek, Mahmut Ozacar, I. Ayhan Sengil, Adsorption of Lead onto Formaldehyde or Sulphuric acid treated Acorn Waste: Equilibrium and Kinetic Studies, *Biochemical Engineering Journal*, 37 **(2007)** 192-200

[14] Slejko F, Adsorption Technology: A step by Approach to Process Calculation and Application (Marcel Decker New York) **(1985)**

[15] Deepak Yadav, Meghna Kapur, Pradeep Kumar, Monoj Kumar Mondal, Adsorptive removal of phosphate from aqueous solution using rice husk and fruit juice residue, *Process Safety and Environmental Protection,* 482 **(2014)** 1-8

[16] Lahieb Faisal Muhaisen, Lemon Peel as Natural Biosorbent to Remove Phosphate from Simulated Wastewater, *Journal of Engineering and Development,* 20 **(2016)** 163 – 173

[17] G. N. Soumya, N. Manickavasagam, P. Santhanam and S. Dinesh Kumar and B. Prabhavathi, Removal of Phosphate and Nitrate from Aqueous solution using Seagrass *Cymodocea rotundata* Beads, *African Journal of Chemistry*, 14 **(2015)** 1393 - 1400

[18] Wasse Bekele, Gezahegn Faye and Nestor Fernandez, Removal of Nitrate ion from Aqueous Solution by Modified Ethiopian Bentonite Clay, *International Journal of Research in Pharmacy and Chemistry*, 4 **(2014)** 192 – 201.

[19] G. N. Soumyaa, N. Manickavasagama, P. Santhanamb and S. Dinesh Kumarb, Efficacy of Seagrass Cymodocea Rotundata Beads on the Removal of Excessive Nutrients in Shrimp Aquaculture Wastewater, *Biological Methods of water Treatment,* 39, **(2017)** 250 – 255

[20] Hakan Demiral, Gül Gündüzoglu, Removal of Nitrate from Aqueous Solutions by Activated Carbon prepared from Sugar Beet Bagasse, *Bioresource Technology*, 101 **(2010)** 1675–1680

[21] Paula Szymczyk1, Urszula Filipkowska1, Tomasz Jóźwiak1, Małgorzata Kuczajowska-Zadrożna, Phosphate Removal from Aqueous Solutions by Chitin and Chitosan in Flakes, *Progress on Chemistry and Application of Chitin and its Derivatives,* XXI **(2016)** 192 – 202

[22] Mahatheva Kalaruban, Paripurnanda Loganathan, W.G. Shim, Jaya Kandasamy, H.H. Ngo, Saravanamuthu Vigneswaran, Enhanced removal of nitrate from water using amine-grafted agricultural wastes, *Science of the Total Environment,* 565 **(2016)** 503 – 510

[23] Shunli Wan, Jiayu Wu, Feng He, Shanshan Zhou, Rui Wang, Bin Gao, Phosphate Removal by lead-exhausted Bioadsorbents simultaneously achieving Lead Stabilization, *Chemosphere,* 10 **(2016)** 1-8

[24] Wondalem Misganaw Golie, Sreedevi Upadhyayula, An investigation on biosorption of nitrate from water by chitosan based organic-inorganic hybrid biocomposites, *International Journal of Biological Macromolecules,* 16 **(2017)** 1 – 47

[25] M. Morghi, F. Abidar, A. Soudani, M. Zerbet, M. Chiban, H. Kabli and F. Sinan, Removal of nitrate ions from aqueous solution using chitin as natural adsorbent, *International Journal of Research in Environmental Studies*, 2 **(2015)** 8 – 20

[26] Mohammad Hassan Shahmoradi1, Behnoush Amin Zade, Ali Torabian and Mahdi Seyed Salehi, Removal of Nitrate from Ground Water using Activated Carbon prepared from Rice Husk and Sludge of Paper Industry Wastewater Treatment, *ARPN Journal of Engineering and Applied Sciences,* 17 **(2015)** 7856 – 7863

[27] G.V. Krishna Mohan, A. Naga Babu, K. Kalpana and K. Ravindhranath, Zirconium-Treated Fine Red Mud Impregnated in Zn-Alginate Beads as Adsorbent in Removal of Phosphate from Water, *Asian Journal of Chemistry*, 29 **(2017)** 2549 – 2558

[28] Ali Gundogdu, Duygu Ozdes, Celal Duran, Volkan Numan Bulut, Mustafa Soylak, Hasan Basri Senturk, Biosorption of Pb (II) ions from aqueous solution by pine bark (Pinus brutia Ten.), *Chemical Engineering Journal.* 153 **(2009)** 62-69

[29] Y.S. Ho, G. McKay, Kinetic models for the sorption of dye from aqueous solution by Wood, *Journal of Environmental. Science. Health Part B: Process Safety Environmental Protection* 76 **(1998)** 183–191

[30] Ru-Ling T Seng, Feng-Chin Wu, Ruey-Shin Juang, Liquid-phase adsorption of dyes and phenols using pinewood-based activated carbons, Carbon. 41 **(2003)** 487-495

[31] Xin Liu, Lingfan Zhang, Removal of Phosphate Anions using the Modified Chitosan Beads: Adsorption kinetic, Isotherm and Mechanism studies, *Powder Technology*, 15, **(2015)** 1-42

[33] Silke Schiewer, Ankit Balaria, Biosorption of Pb2+ by original and protonated citrus peels: Equilibrium, kinetics and mechanisms, *Chemical Engineering Journal*, 146 **(2009)** 211-219

[34] B Stephen Inbaraj, N Sulochana, Mercury adsorption on a carbon sorbent derived from fruit shell of Terminalia catappa, *Journal of Hazardous Materials*, 133 **(2006)** 283-290.

[35] M. Horsfall Jr., A.A. Abia, A.I. Spif, Kinetic studies on the adsorption of Cd2+, Cu2+ and Zn2+ ions from aqueous solutions by cassava (Manihot sculenta Cranz) tuber bark waste, *Bioresource Technology* 97 **(2006)** 283–291

[36] Carlos Green- Ruiz, Mercury(II) removal from aqueous solutions by nonviable Bacillus sp. from a topical estuary, *Bioresource Technology*, 97 **(2006)** 1907-1911

[37] B. Das, N. K. Mondal, R. Bhaumik, P. Roy, Insight into adsorption equilibrium, kinetics and thermodynamics of lead onto alluvial soil, *International Journal of Environmental Science and Technology*, **(2014)** 11:1101–1114

[38] E. Igberase, P. Osifo, and A. Ofomaja, The Adsorption of Pb, Zn, Cu, Ni, and Cd by Modified Ligand in a Single Component Aqueous Solution: Equilibrium, Kinetic, Thermodynamic, and Desorption Studies, 2017 **(2017)** 1-15

[39] Ozgul Gercel, H. FerdiGercel, Adsorption of Lead(II) ions from Aqueous Solutions by Activated Carbon Prepared from Biomass Plant Material of Euphorbia Rigida, *Chemical Engineering Journal*, 132 **(2007)** 289-297

[40] Ru-Ling T Seng, Feng-Chin Wu, Ruey-Shin Juang, Liquid-Phase Adsorption of Dyes and Phenols using Pinewood-based Activated Carbons, *Carbon*, 41 (**2003)** 487-495.

[41] C.W. Cheung, J.F. Porter, G. McKay, Sorption Kinetic Analysis for the Removal of Cadmium ions from Effluents using Bone Char, *Water Research*, 35 **(2001)** 605-612.

[42] H. Thagira Banu, P. Karthikeyan, Sankaran Meenakshi, $Zr^{4+}$ ions embedded Chitosan-Soya Bean Husk Activated Bio-char Composite Beads for the Recovery of Nitrate and Phosphate ions from aqueous solution, *International Journal of Biological Macromolecule*, 18 **(2019)** 1 – 44

[43] V.M. Tangde, S.S. Prajapati, B.B. Mandal, N.P. Kulkarni, Study of Kinetics and Thermodynamics of removal of Phosphate from Aqueous using Activated Red Mud, *International Journal of Environmental Research*, **(2017)**

[44] Hassan A Hanafi and sami M Abdel Azeema, Removal of Nitrate and Nitrite Anions from Wastewater using Activated Carbon Derived from Rice Straw, *Journal of Environmental and Analytical Toxicology*, 6 **(2016)** 1 – 6.